Machining Science and Technology, 9:567–588

ISSN: 1091-0344 print/1532-2483 online
DOI: 10.1080/10910340500398233

Taylor & Francis
Taylor & Francis Group

INDUCTION-HEATED TOOL MACHINING OF ELASTOMERS — PART 2: CHIP MORPHOLOGY, CUTTING FORCES, AND MACHINED SURFACES

Jie Luo, Hongtao Ding, and Albert J. Shih □ *Department of Mechanical Engineering, University of Michigan, Ann Arbor, Michigan, USA*

□ *The induction-heated tool and cryogenically cooled workpiece are investigated for end milling of elastomers to generate desirable shape and surface roughness. Elastomer end milling experiments are conducted to study effects of the cutting speed, tool heating, and workpiece cooling on the chip formation, cutting forces, groove width, and surface roughness. At high cutting speed, smoke is generated and becomes an environmental hazard. At low cutting speeds, induction heated tool, if properly utilized, has demonstrated to be beneficial for the precision machining of elastomer with better surface roughness and dimensional control. Frequency analysis of cutting forces shows that the soft elastomer workpiece has low frequency vibration, which can be correlated to the surface machining marks. The width of end-milled grooves is only 68 to 78% of the tool diameter. The correlation between the machined groove width and cutting force reveals the importance of the workpiece compliance to precision machining of elastomer. This study also explores the use of both contact profilometer and non-contact confocal microscope to measure the roughness of machined elastomer surfaces. The comparison of measurement results shows the advantages and limitations of both measurement methods.*

Keywords Elastomer Machining, Induction-Heated Tool, Chip Morphology, Machined Surfaces

INTRODUCTION

Effective removal of the elastomer material by machining to generate the precise shape and desired surface roughness of the workpiece is technically challenging due to the unique properties of very low elastic modulus and large elongation before fracture of work-material (1). A series of elastomer end-milling tests has been conducted. Test results demonstrated benefits of the sharp, down-cut tool, cryogenically cooling the workpiece, and consistent workpiece fixturing on the effectiveness of work-material

Address correspondence to Albert J. Shih, Department of Mechanical Engineering, University of Michigan, Ann Arbor, MI 48109, USA. E-mail: shiha@umich.edu

removal, chip morphology, and cutting forces (1, 2). Induction-heated tool (3) is a new approach that can potentially improve the precision and surface roughness for elastomer machining. High tool temperature can soften the elastomer workpiece in front of the cutting edge and enable more effective tool penetration and chip formation.

Cutting speed is a key factor in elastomer machining. As observed by Jin and Murakawa (4), high cutting speed generates good surface roughness in elastomer machining. This observation is confirmed in this study. However, at high cutting speed, smoke is generated due to the burning of elastomer chips. It becomes an environmental and health hazard and limits the cutting speed in elastomer machining. Low but effective cutting speed is desirable for elastomer machining. Under this constraint, the induction-heated tool could be beneficial. In this study, effects of three key machining process parameters, the cutting speed, tool heating, and workpiece cooling, are investigated for the end milling of the KM rubber, a natural rubber compound provided by Michelin for automotive tire tread applications. The KM rubber consists mostly of the natural rubber. Properties of the natural rubber compound can be used to represent the work-material (5).

The chip morphology in elastomer machining is unique. Material properties of the elastomer, such as the very low thermal conductivity and elastic modulus and the large elongation before fracture (2) all contribute to distinctively different shapes of machined chips. A four-step procedure, as shown in Figure 1, has been proposed to classify the morphology of elastomer chips (2). Based on four classification steps, i.e., burning, straight or rough edge, curl or flat shape, and serrated or smooth surface, seven types of elastomer chip can be identified. In this study, this procedure was applied to classify elastomer chips generated in end milling tests.

The accurate measurement to quantify the roughness of machined elastomer surface is a technical challenge. Using the contact stylus method, fine features and asperities on the elastomer surface are deformed by the

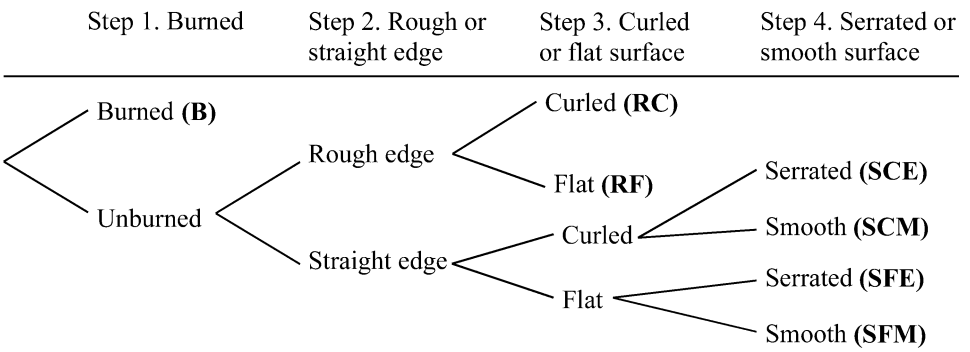

FIGURE 1 Four-step procedure to classify chip morphology for elastomer chip (2).

contact force. This has been discussed by Stupak et al. (6) using the profilometer to characterize the worn surface of rubber. Using the non-contact optical method, the low reflectivity of the surface is a problem. Elastomers for tire applications, like the workpiece used in this study, are usually black and have very low light reflectivity. Ganesan et al. (7) and Schaal and Coran (8) explored the quantitative measurement of elastomer surface by the optical image processing technique but did not correlate measured results to commonly used surface roughness parameters. In this study, the confocal scanning microscopy, which has been used extensively for the measurement of soft tissue and biological materials (9), was applied to study the roughness of machined elastomer surfaces. The height at a small, 1 μm diameter region can be determined by detecting the intensity peak of the laser light reflected from the surface. A confocal scanning microscope with 64 sensors for rapid measurement is used in this study. Roughness measurements using both the contact stylus profilometer and non-contact confocal microscopy are compared in this study.

Cutting forces provide the insight of the interaction between the tool and workpiece in machining. The research conducted by Shih et al. (2) shows that end milling of solid carbon dioxide cooled elastomers, compared to the room temperature workpiece, generated larger cutting forces. By studying the cutting forces, effects of three key process parameters (cutting speed, tool heating, and workpiece cooling) are investigated. The groove width after end milling of elastomer is significantly smaller, about 22 to 32% less, than the tool diameter. This is due to the low elastic modulus and large deformation of the elastomer workpiece exhibited during machining. The correlation between the groove widths and cutting forces is studied. The elastomer workpiece can also vibrate during machining at a low frequency, likely also at a relatively large amplitude. Frequency analysis of the cutting forces can reveal the vibration of elastomer workpiece and correlate with the distance between machining marks.

The experimental setup, test procedure, and data analysis are presented in the following section. The size and morphology of elastomer chip are classified. Cutting force analysis and width of machined grooves are presented. The measurement results and quantitative analysis of machined surfaces are discussed in the final section.

EXPERIMENT SETUP, TEST PROCEDURE, AND DATA ANALYSIS

Machine Setup

The experimental setup for end milling of elastomers is shown in Figure 2. The tool, a 12.7 mm diameter, 127 mm long, double-flute, down-cut high speed steel end mill (Onsrud 40-series), was driven by the

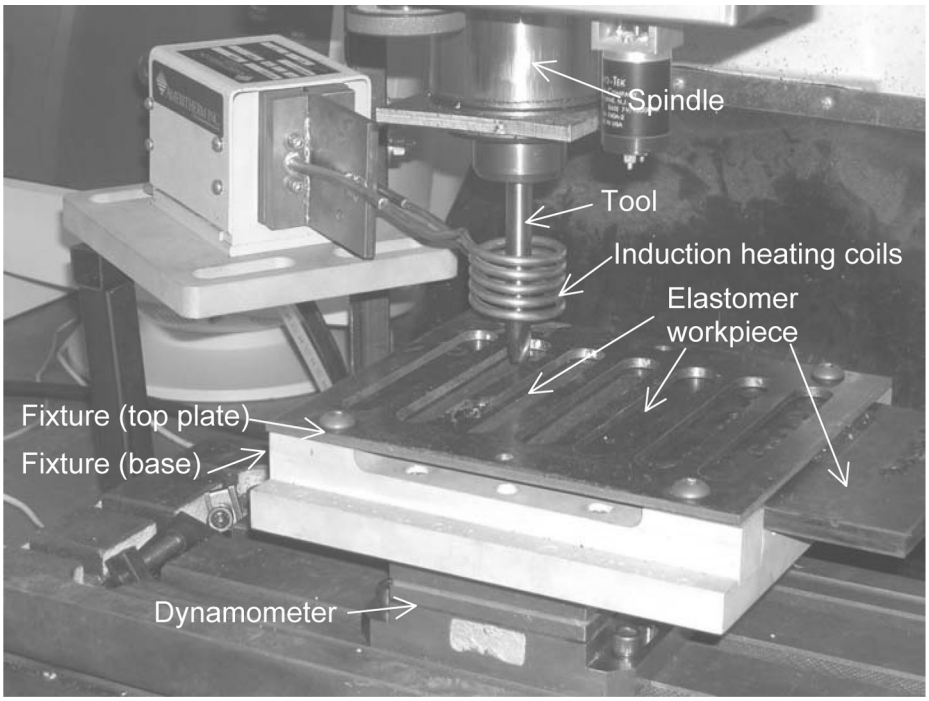

FIGURE 2 Experimental setup of elastomer end milling with tool induction heating.

spindle in a CNC vertical end milling machine. This is the same tool used in the induction heating experiments (3). The tool geometry has proven to be effective in the elastomer material removal in end milling (1). A Ti-6Al-4V thermal insulator was used to reduce the heat transfer to the spindle (3). A water-cooled induction heating coil surrounding the tool could be utilized to heat the rotating tool for elastomer machining.

Good fixture design is important for elastomer machining (1). The fixture, as shown in Figure 2, is designed to hold the plate-shape elastomer workpiece between the base and top plate. There are seven grooves on the top plate for seven end milling tests along these grooves. This fixture design can provide adequate and consistent structural support to the soft elastomer workpiece for end-milling experiments. The fixture was mounted on a force dynamometer.

Experimental Design

Eight elastomer end milling tests were conducted at two spindle speeds (1100 and 2400 rpm), two tool temperatures (with and without induction heating to 300°C tool tip temperature), and two workpiece temperatures

TABLE 1 Tool and Workpiece Temperatures in Four End-Milling Experiments

	Room temperature tool (23°C)	Induction-heated tool (300°C)
Room temperature workpiece (23°C)	Exp. I	Exp. II
Solid carbon dioxide cooled workpiece (–78°C)	Exp. III	Exp. IV

(with and without cooling by solid carbon dioxide at −78°C) to study effects of three process parameters. The feed rate was 3 mm/s and depth of cut was 4 mm. All tests were conducted dry without cutting fluid. As shown in Table 1, four sets of experiments, marked as Exp. I, II, III and IV, are used to classify these eight cutting tests by the tool and workpiece temperatures. For each elastomer end milling test, chips were collected, cutting forces were recorded, width of grooves was measured, and machined surfaces were inspected.

Surface Inspection

Comprehensive study of machined elastomer surfaces using the contact stylus profilometer, confocal scanning microscopy, scanning electron microscopy (SEM), and optical microscopy were performed in this study. The arithmetical average roughness, R_a, was selected as the parameter to represent the machined elastomer surface. The cutoff length for filtering the raw measurement data is critical to obtain representative and consistent R_a values. The upper and lower cut-off lengths of the Gaussian filter are applied to derive the roughness of the profile (10). The conventional upper cutoff length of 0.8 mm is not suitable for machined elastomer surfaces due to the large distance between machining marks at low spindle speed. In this study, 2.5 mm upper cutoff length was selected to meet the general guideline to have about 10 surface high points within the upper cutoff length (11).

A Taylor-Hobson profilometer with the sharp 10 μm radius tip was utilized for the contact stylus measurement. Two 40 mm traces were conducted along and against the milling feed direction (5). These two measurement results were averaged. The profilometer had a lateral resolution of 1 μm.

The Siemens SISCAN MC64 confocal scanning microscope with 440 μm measurement range and 0.5 μm height and 10 μm lateral resolutions was applied for the non-contact measurement of machined elastomer surfaces. This optical measurement device used an infrared diode laser with 830 nm wavelength to scan 200 traces (6 mm long) in a 2 mm by 6 mm area. This confocal microscope had 64 sensors for fast and precise scanning measurement.

The low reflectivity of black elastomer material can cause the high frequency noise in confocal microscope measurements. A 6 mm long measurement on the elastomer surface machined in Experiment IV (with tool heating and workpiece cooling) at 2400 rpm is shown in Figure 3(a) as an example. High spikes, which exceed the 440 μm measurement range, can be seen. The high frequency noise can be removed using software filtering methods.

Frequency domain analysis of all eight confocal microscope measurements showed a peak at about 20 μm wavelength due to the high frequency noise. The finite impulse response (FIR) low pass filter in MATLAB with the stop wavelength of 25 μm and pass wavelength of 50 μm was used to

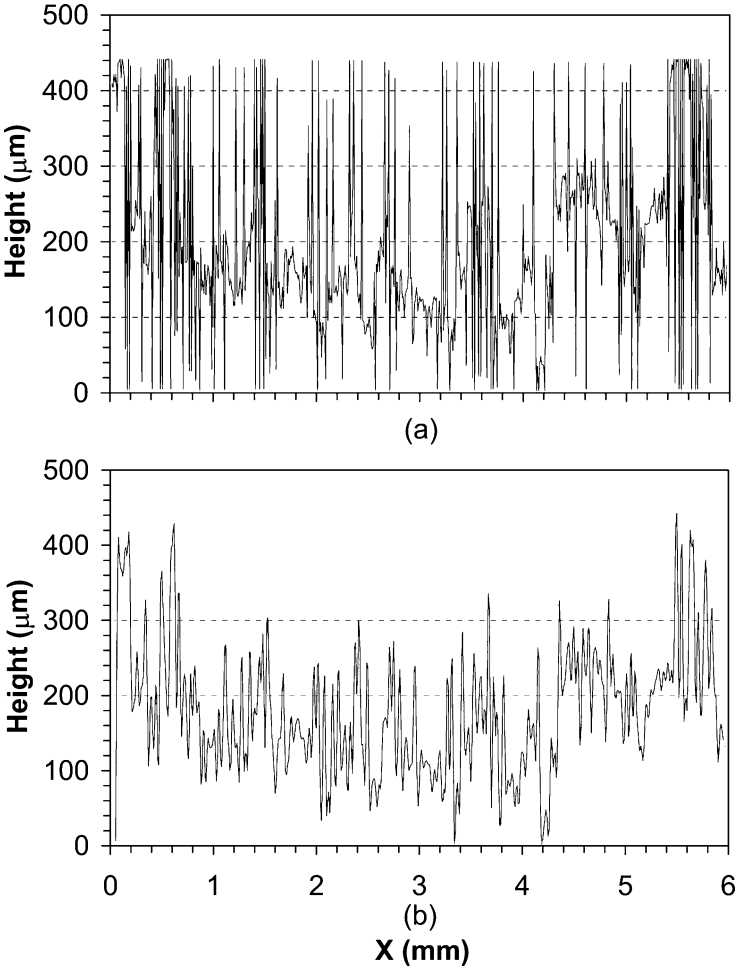

FIGURE 3 Height profile of machined surface generated in Experiment IV at 2400 rpm: (a) the original height profile, and (b) the height profile with high-frequency noises filtered.

remove the high frequency noise. The measured data in Figure 3(a) was processed using the FIR filter and results are shown in Figure 3(b). The high frequency noise is removed.

Another method was using the Gaussian filter in OmniSurf, a surface texture software package produced by Digital Metrology Solutions, Inc. The lower cutoff length of the Gaussian filter was set at 25 μm to remove the high frequency noise. Omnisurf was used to analyze both the contact stylus and optical confocal microscope measurement data and extract the R_a value.

A Philips XL SEM was used to observe the machined elastomer surfaces.

Force Analysis

A piezoelectric force dynamometer, Kistler Model 9257B, as illustrated in Figure 2, was used to measure the three force components during elastomer end milling tests. The voltage signals from the dynamometer were amplified and acquired using a PC-based data acquisition system at 1000 Hz sampling rate. Calibration tests were conducted to find the conversion factor from voltage to force. The XYZ coordinate system used to define the cutting force direction is shown in Figure 4. The X-axis coincides with the feed direction. The Z-axis is along the rotating axis of the tool, which is perpendicular to and pointing outward from the flat surface of elastomer plate.

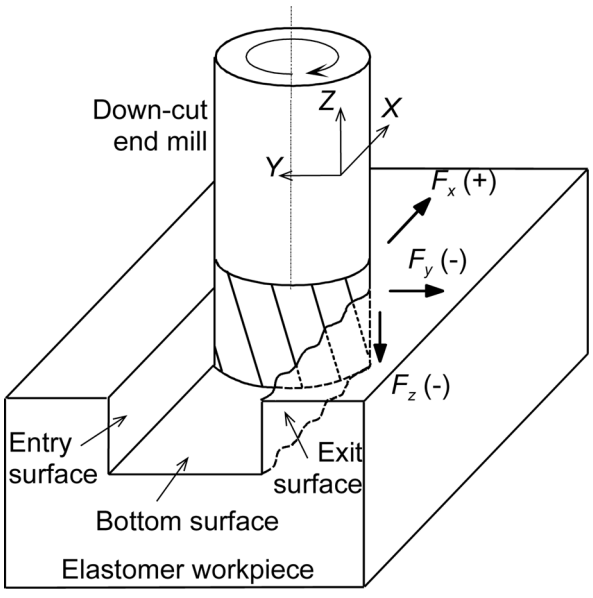

FIGURE 4 End-milling force components.

F_x, F_y, and F_z are three end-milling force components acting on the workpiece from the rotating tool. The F_x should generally be positive because of the tool feed direction. Due to the rotational direction of the tool, the F_y should be mostly negative. Since the tool pushes the workpiece in the negative Z direction, F_z should remain negative. Such trends have been demonstrated in Reference (2) and also observed in this study. For each revolution of the double-flute tool, two peaks occurred in traces of force components F_x and F_y (2).

CHIP SIZE AND MORPHOLOGY

Figure 5 shows the optical micrographs of elastomer chips for Exps. I to IV. Four types of chips, B, RC, SCM, and RF, with the size ranging from 1–2 to 5–7 mm are identified. The uncut length and width of the chip is 19.9 and 4 mm, respectively, for the 12.7 mm diameter tool used in this study. The actual size of the chip is much smaller. This indicates the frequent breakage of chip during end milling.

At high temperature, the elastomer degrades and gasifies into smoke. The vulcanized natural rubber compound begins to degrade around 150 to 200°C (12). This is lower than the 300°C tip temperature of the induction heated tool. During cutting, the high localized temperature in chip burns a portion of the elastomer material, generates smoke, and creates the B type chip morphology with the melting surface texture. Higher chip temperature is expected at high spindle speed, induction heated tool, and room temperature workpiece. This can be validated by observing the high concentration of B type chip in Figure 5.

The effect of cutting speed can be identified that, at 1100 rpm spindle speed, only the induction heated tool has the B type chip. At 2400 rpm spindle speed, all four cutting tests have the burned, B type chip. Under the same tool feed rate, the high spindle speed reduces the maximum uncut chip thickness and increases the specific energy input to the elastomer chip. This promotes the chip burning and B type chip formation. All four tests at 2400 rpm spindle speed also generate visible smoke during end milling tests. The effect of cryogenic workpiece cooling on B type chip generation is not as obvious as the spindle speed and tool heating. Close observation of chips can recognize that, although not obvious, less concentration of the B type chip for cutting the cryogenically cooled elastomer workpiece.

The RC and SCM types chip morphology can be seen in all cutting conditions except the induction-heated tool cutting without workpiece cooling (Exp. II) at 2400 rpm spindle speed, which is the setup with the highest specific energy input to the elastomer workpiece. Under such cutting condition, the RF type chip, small chip size, and high concentration of B type chip are recognized. The elongation before fracture of elastomer

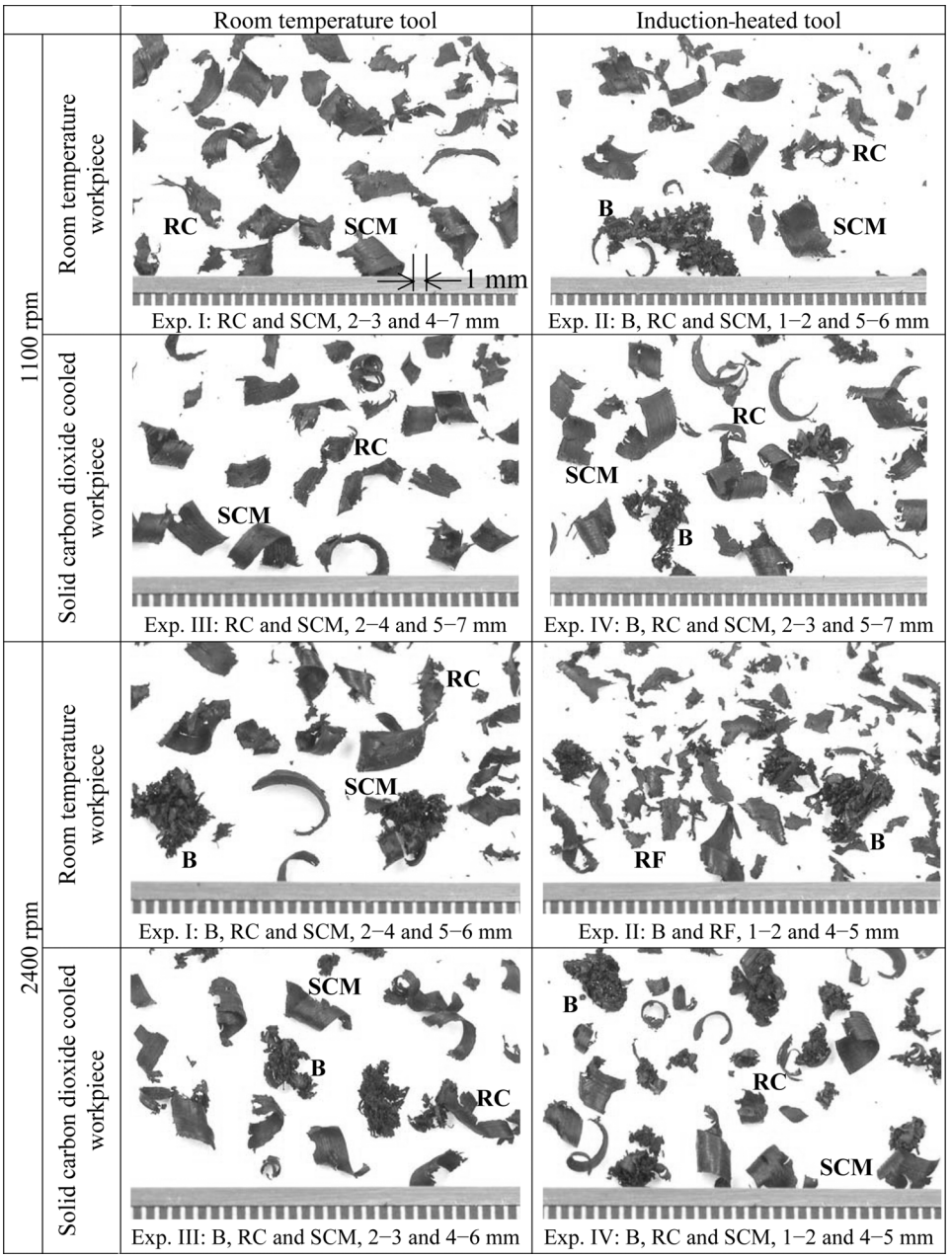

FIGURE 5 Optical micrographs of elastomer chips.

is reduced at elevated temperature (13). Also, at high strain rate, the elastomer becomes less ductile (14). Both material properties contribute to more frequent chip breakage and facilitate the RF type of chip

generation. Under the same initial tool and workpiece temperatures, higher concentration of small size chip can be found at the 2400 rpm spindle speed in all four Exps. I to IV. It is particularly obvious in Exp. II.

CUTTING FORCES

Figure 6 shows three end milling force components, F_x, F_y, and F_z, and the frequency domain analysis of F_x and F_y in Exp. II (induction-heated tool, no workpiece cooling) at 1100 rpm spindle speed. As expected, F_x remains mostly positive and F_y, and F_z remain negative during end milling (2). The F_x and F_y show the significant cyclic variation due to the tool rotation while the F_z remains at a relative constant level of about –90 N. For each revolution of the tool (0.055 s), two peaks can be seen in F_x and F_y for the double flute tool (2). Similar trend of F_x, F_y, and F_z can be observed for end milling at 2400 rpm. This is illustrated by an example of Exp. IV (induction-heated tool with workpiece cooling) in Figure 7(a).

The frequency domain analysis of Exp. II at 1100 rpm, as shown in Figure 6(b), shows the peak frequency at 37.1 Hz, which is twice of the 1100 rpm spindle speed because of the double-flute tool. Another two peaks observed in F_y are at 18.6 Hz (the 1100 rpm spindle speed) and 6.8 Hz. As shown in Figure 7(b), at 2400 rpm spindle speed, a peak at the same 6.8 Hz can also be identified along with 40.5 Hz (2400 rpm) and 81.0 Hz (twice the spindle speed for double-flute tool). Table 2 summarizes the frequency of the 1st, 2nd, and 3rd peaks of F_y for eight end milling tests. All eight tests, regardless of spindle speed, have the 1st peak frequency at about 7 Hz. This relatively low frequency is due to the vibration of the soft elastomer workpiece.

This low 7 Hz frequency vibration can be recognized in the time domain force traces in Figures 6(a) and 7(a). In Figure 6(a), high peaks of F_y are marked by the thick arrows. Spacing between these arrows is about every 6 peaks or 3 revolutions of the tool at 1100 rpm. This matches to the 7 Hz frequency. At 2400 rpm, the 7 Hz frequency corresponds to about 6 tool revolutions or 12 spacing between high peaks of F_y. This can also be recognized by two thick arrows in Figure 7(a). The workpiece low frequency vibration has a significant effect on the machining marks or surface texture generation at 1100 rpm spindle speed. As will be presented by SEM micrographs of machined surfaces seen later, the distance between machining marks is affected by the workpiece low frequency vibration.

It is noted that there are discrepancies between the actual measured peak frequencies and speed settings: 1100 rpm (18.3 Hz) and 2400 rpm (40.0 Hz). This is due to the accuracy of the machine spindle speed control and also possibly affected slightly by the frequency analysis calculation.

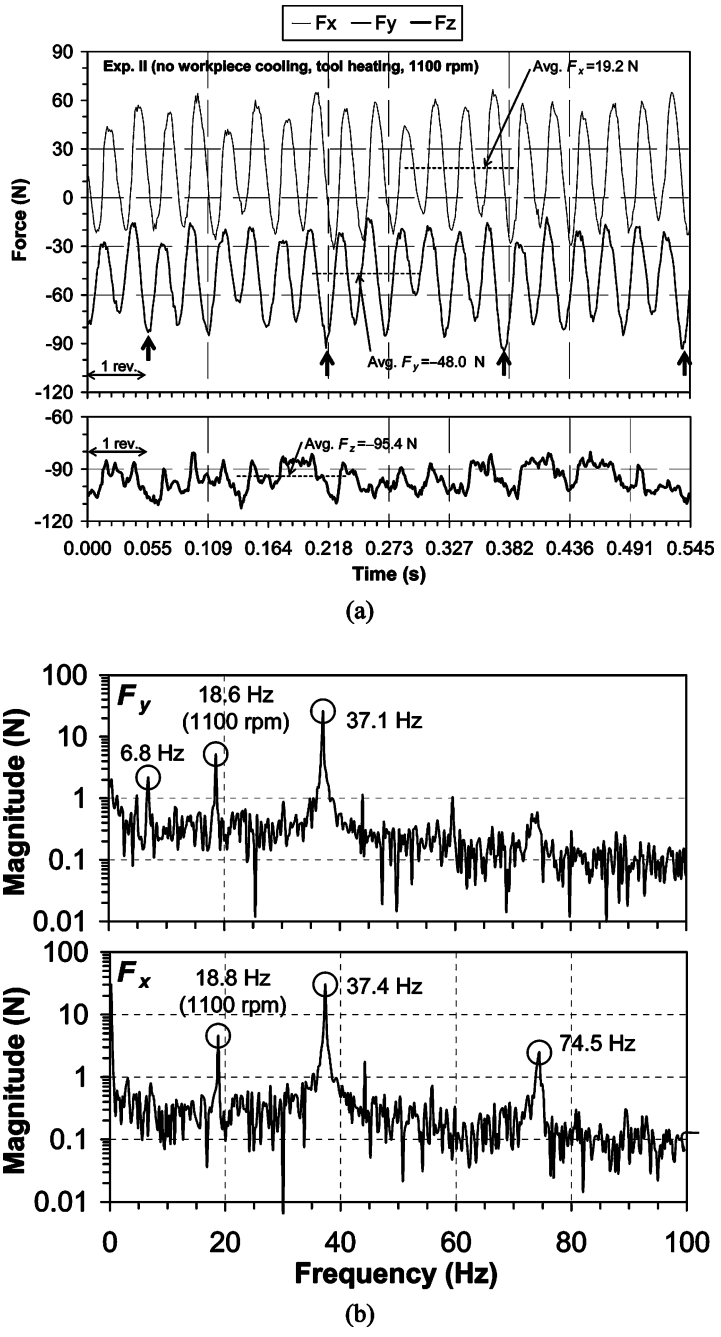

FIGURE 6 Experiment II (no workpiece cooling, tool heating, 1100 rpm): (a) three end-milling force components vs. time, and (b) frequency domain analysis.

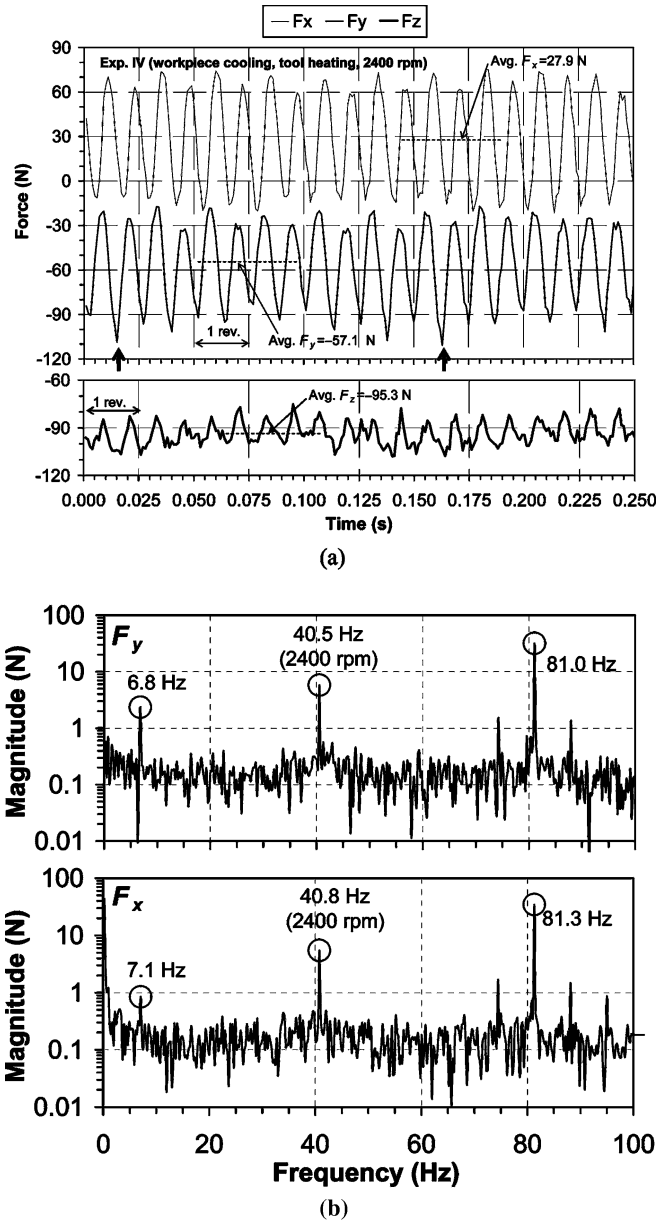

FIGURE 7 Experiment IV (workpiece cooling, tool heating, 2400 rpm): (a) three end-milling force components vs. time, and (b) frequency domain analysis.

Effects of spindle speed, tool heating, and workpiece cooling on the magnitude of the averaged peak cutting forces are presented in Figure 8. The averaged peak cutting force components F_x, F_y, and F_z are calculated

TABLE 2 Peak Frequency of F_y in Elastomer End-Milling Experiments

		Peak frequency (Hz)					
		Room temperature tool			Induction-heated tool		
Spindle speed (rpm)	Workpiece temperature	1st	2nd	3rd	1st	2nd	3rd
1100	Room temperature	7.1	18.6	36.9	6.8	18.6	37.1
	Solid carbon dioxide cooled	6.8	18.5	37.1	7.1	18.6	37.1
2400	Room temperature	6.8	40.5	81.4	7.1	40.8	81.3
	Solid carbon dioxide cooled	6.8	40.8	81.3	6.8	40.5	81.1

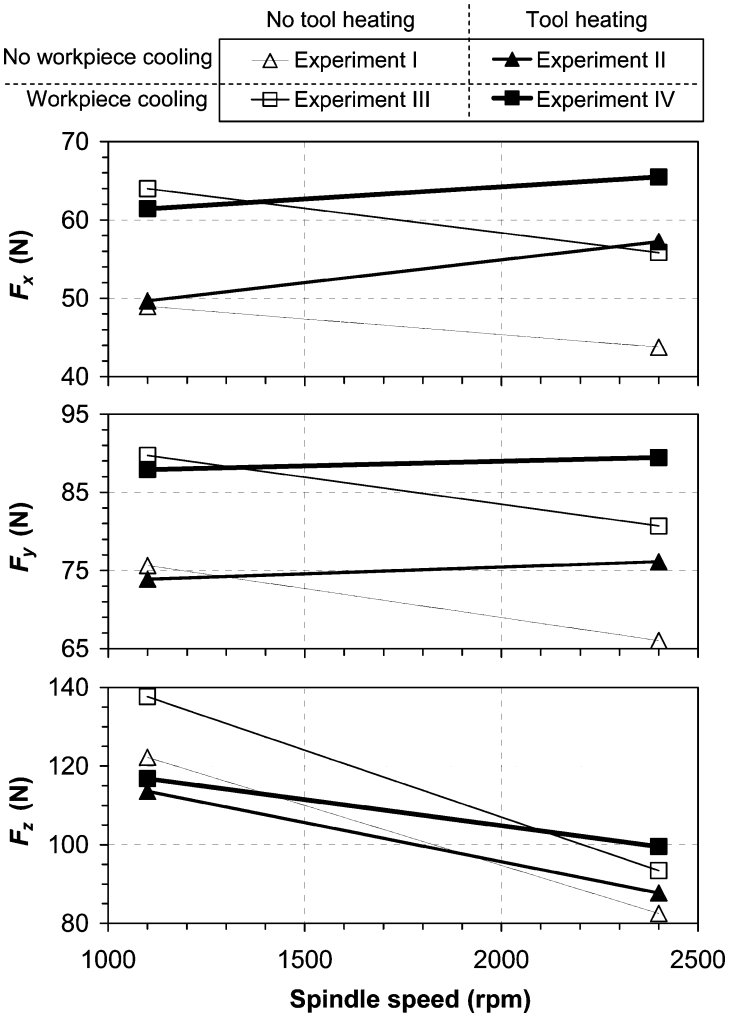

FIGURE 8 Averaged peak values of end-milling forces vs. spindle speeds.

by averaging the absolute value of 120 consecutive peaks in 60 tool rotations (2).

The effect of spindle speed on cutting forces depends on tool heating condition. At high spindle speed, the uncut chip thickness is reduced, which is expected to decrease the cutting forces, and the strain rate is increased, which, in turn, will increase the cutting forces. With tool heating (solid symbols in Figure 8), cutting forces F_x and F_y increase at higher spindle speed. This is likely due to the adhesion of elastomer work-material to the tool rake surface and changes of cutting edge geometry similar to the build-up edge in metal cutting (15). With the combination of high cutting speed and heated tool, the build-up edge for elastomer machining is created and results in high cutting forces. The build-up edge is visible on the tool cutting edge after end milling. This tool requires cleaning at the beginning of end-milling tests. With no tool heating (open symbols in Figure 8), minimal chip adhesion or no build-up edge was observed and lower cutting forces F_x and F_y can be seen at 2400 rpm spindle speed. Regardless of tool temperature and workpiece cooling, smaller F_z is generated at 2400 rpm spindle speed. At 1100 rpm spindle speed, tool heating does not change cutting forces significantly. The effect of tool heating on cutting forces becomes apparent at the high spindle speed. On the workpiece cooling effect, higher cutting forces can be identified with cryogenically cooled workpiece. This is consistent with the observation in (2).

MACHINED GROOVES

The optical pictures of the groove and bottom surface of machined elastomer workpiece in all end milling tests are shown in Figure 9. The arc of machining marks with its curvature resembling the tool diameter can be recognized on bottom surfaces of the groove at low spindle speed (1100 rpm). At 2400 rpm, the curved machining marks can be seen only on the workpiece without cryogenic cooling. For the solid carbon dioxide cooled workpiece machined at 2400 rpm, the bottom surface of groove does not have clearly visible curved machining marks. Using SEM, machined surfaces will be further investigated in the following section.

Unlike the conventional end milling of metals, the groove width, W, ranging from 8.6 to 9.9 mm and listed in Figure 9, is much narrower than the 12.7 mm tool diameter. This demonstrates the difficulty to generate a precise shape in elastomer machining. The elastomer workpiece is deformed by the cutting forces during machining and recovers afterward. This is illustrated in Figure 10(a) by the picture of a hole generated at the end of a milling trace. While the tool is not moving but continuously rotating and retracting from the workpiece, a hole larger than the groove width but smaller than the tool diameter is generated. Figure 10(b) shows

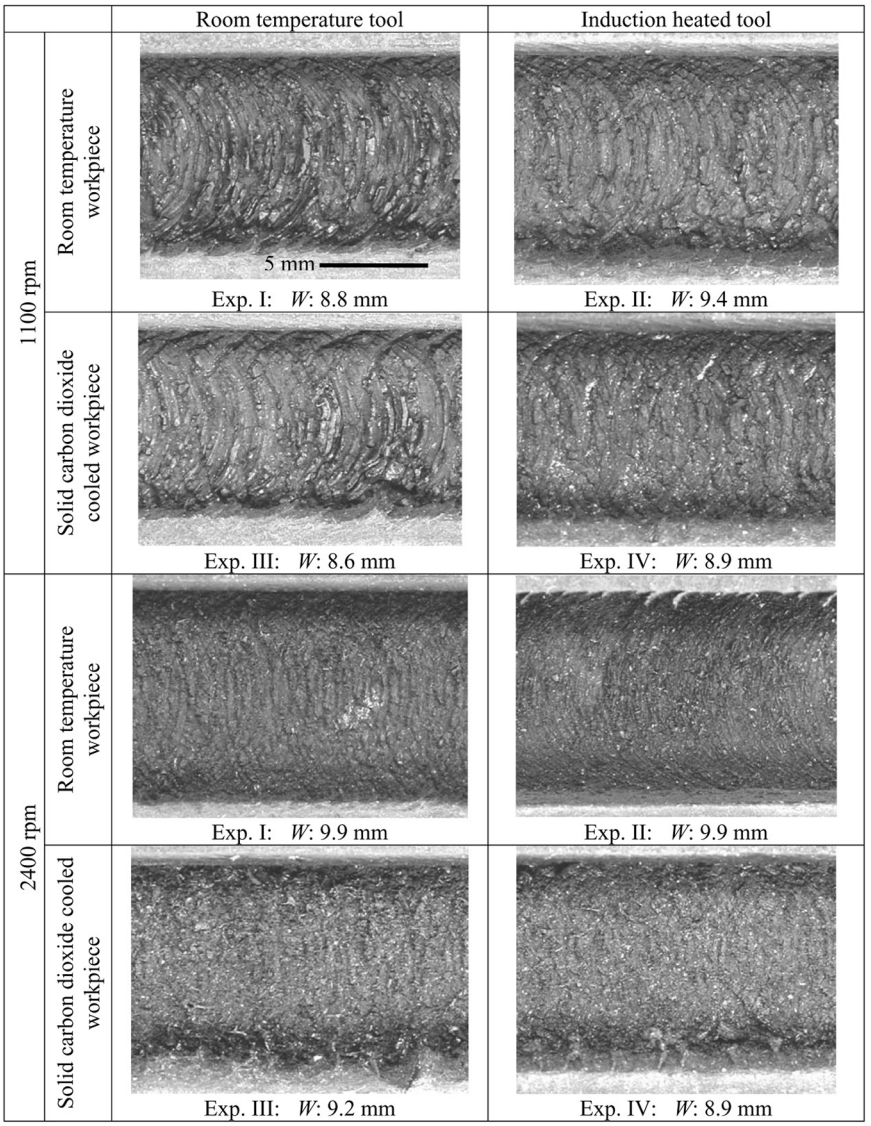

FIGURE 9 Optical pictures of machined surface. (W is the groove width).

relative size of the hole, tool, and maximum and minimum groove width machined in end milling tests. Process parameters significantly affect the groove width as well as the topography of two side surfaces on the groove.

Two side surfaces in the groove are distinctly different. The surface as the tool cuts into the workpiece, marked as the entry surface, is smoother than the opposite side, which is denoted as the exit surface. The exit surface is wavy and often has long residual burrs. Due to the waviness of exit

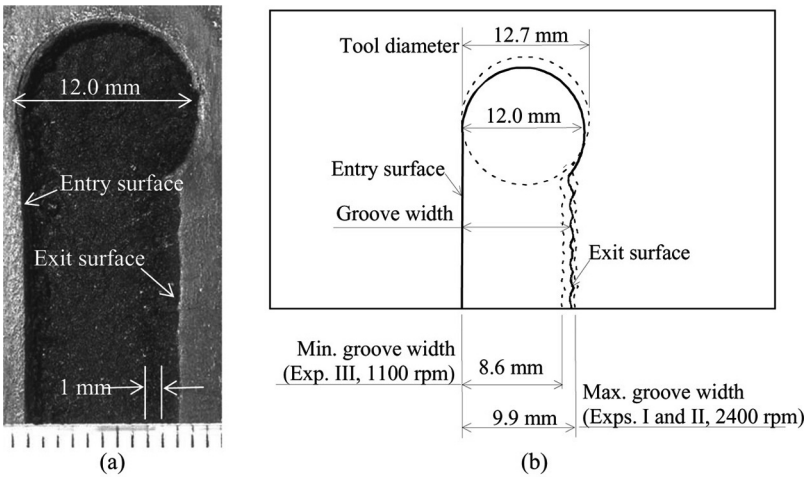

FIGURE 10 Top view of the groove machined in Exp. I at 2400 rpm: (a) picture of the hole generated by retracting end milling tool, and (b) relative size of the tool, hole, and maximum and minimum groove width.

surface, the groove width is measured at 10 locations. The averaged value is used to represent the groove width.

Depending on the cutting conditions, the groove width is only 68 to 78% of tool diameter. The deformation is mainly caused by the compression caused by the cutting force F_y on the workpiece in the Y direction during end milling. The groove width, W, vs. the average F_y of Exps. I to IV is shown in Figure 11. The number next to the symbol indicates the spindle speed, either 1100 or 2400 rpm. The high spindle speed generates wider groove width in all four Exps. I to IV. The maximum groove width, about 9.9 mm, is generated under two cutting conditions (with and without tool heating) at 2400 rpm with no workpiece cooling. Cryogenically cooling the workpiece (square symbols) increases the workpiece elastic modulus but generally does not create a wider groove. This contradicts intuitive thinking and is likely to be caused by the more effective material removal of the elastomer material, even at room temperature, using the sharp, down-cut router tool.

A linear trend can be recognized for data points in Figure 11. The regression analysis is applied to fit a line to eight data points.

$$W = -0.07 \cdot F_y + 12.5 \text{ (mm)} \tag{1}$$

Equation 1 indicates that, as the force F_y approaches 0, the groove width W is 12.5 mm, which is close to the 12.7 mm tool diameter. The coefficient of 0.07 mm/N in Equation 1 is the estimated compliance of workpiece in the

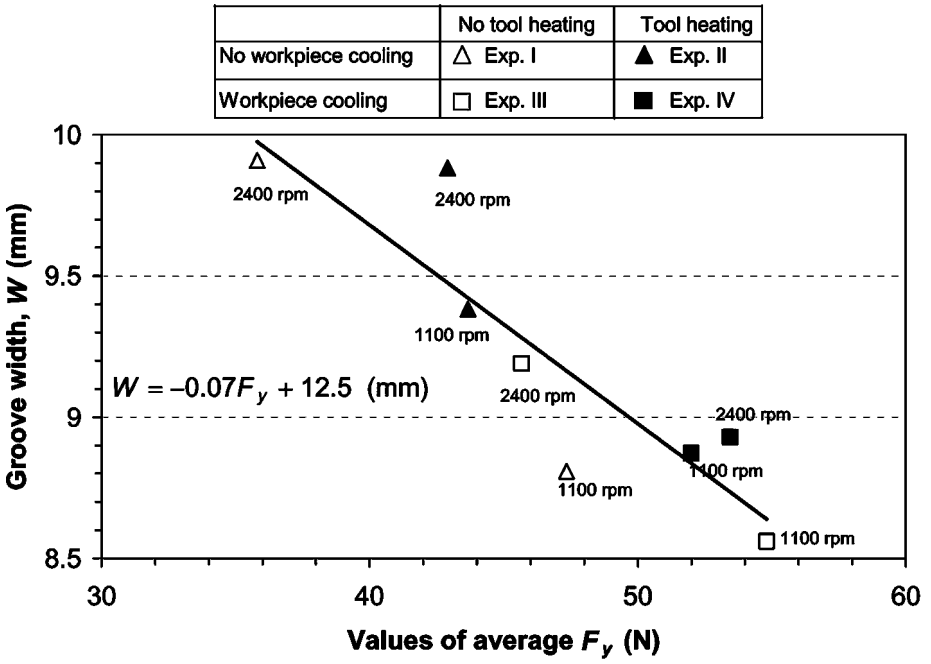

FIGURE 11 Relationship between the groove width W and cutting force F_y.

Y direction under the experimental setup used in this study. Decreasing the workpiece compliance can help reduce the groove width variation. This affirms the previous finding of the importance of fixture design in elastomer machining (1).

MACHINED SURFACES

Bottom surfaces of machined grooves in eight elastomer end milling tests, as shown in Figure 9, are investigated in this section. Figure 12 presents SEM micrographs on corresponding machined surfaces with detailed features such as curved machining marks, burrs, and residuals after burning. The distance between machining marks and surface roughness, measured using both contact and non-contact measurement methods, are discussed in the following sections.

Distance Between Machining Marks

At 3 mm/s feed, the double-flute end mill has 82 and 38 μm maximum uncut chip thickness at 1100 and 2400 rpm spindle speed, respectively (16). Ideally, if a chip is removed in every engagement of the cutting edge and

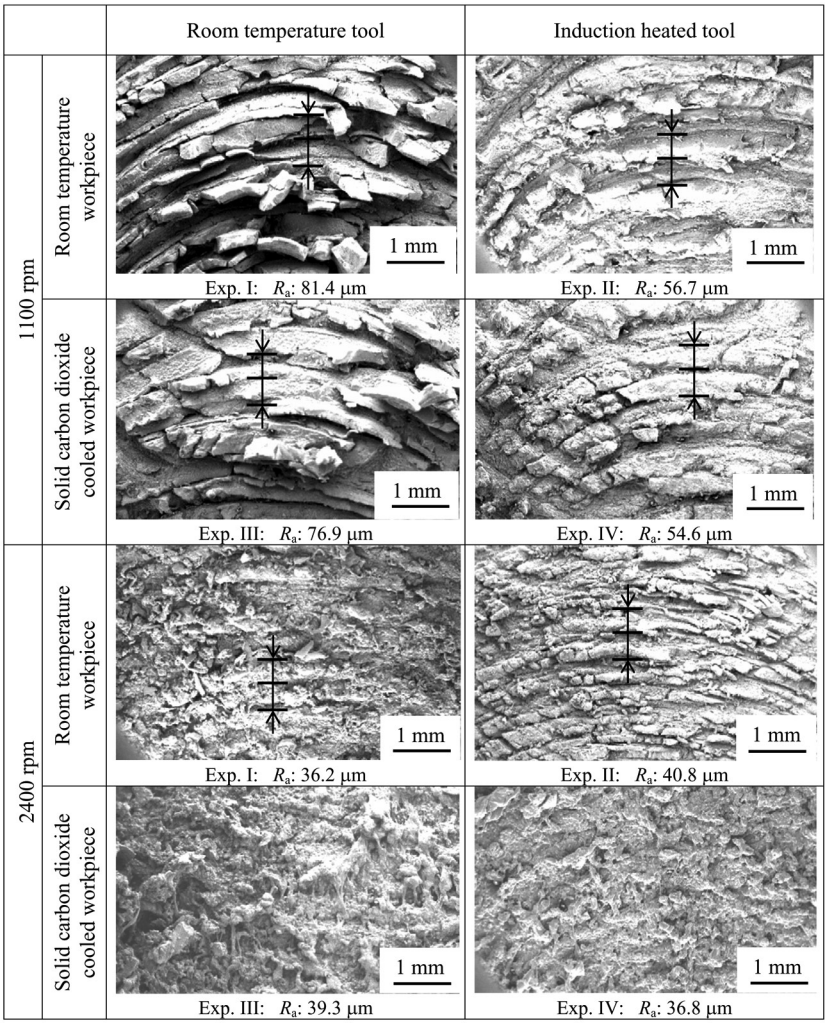

FIGURE 12 SEM micrographs of machined surface. (R_a is measured by the contact stylus profilometer).

workpiece, the distance between machining marks on the machined surface will reflect such value (17). The actual distance, measured from SEM micrographs, between major machining marks is about 0.4 to 0.5 mm. It is much larger than the ideal value and indicates that, during the end milling, the tool cutting edges rub against the elastomer workpiece several times until a critical condition is reached to generate the chip. Between major machining marks, some minor machining marks can be seen. It reveals the source for chip generation during end milling.

At 1100 rpm, the 0.4 to 0.5 mm distance between machining marks, as indicated in Figure 12, is about 6 times of the maximum uncut chip

thickness (82 μm). The distance between three horizontal lines in Figure 12 is 0.45 mm. About 6 engagements of the cutting edge with the workpiece, or 3 revolutions of the double-flute tool, will create a chip removal cutting action. Correspondingly, high peaks of F_y are observed at about every 6 peaks in Figure 6(a). In one period of the workpiece 7 Hz low frequency vibration, which is about 0.14 s, the tool advances 0.43 mm in the feed direction. This value is close to the distance between machining marks and indicates that, at 1100 rpm spindle speed, the workpiece vibration is a key factor on the distance between major machining marks.

At 2400 rpm, machining marks can only be recognized on surfaces machined on workpiece with no cryogenic cooling. This matches to the observation in Figure 9 using the optical microscope. About the same distance (0.4 to 0.5 mm) between major machining marks can be seen as in the 1100 rpm. Under the same workpiece vibration frequency (7 Hz) and feed rate (3 mm/s), the tool advances the same 0.43 mm in the feed direction in one period of workpiece vibration. The effect of workpiece vibration on the distance between machining marks can also be identified on machined surfaces. There are many minor machining marks with much shorter spacing distance on surfaces machined at 2400 rpm. The more efficient cutting at high spindle speed and frequent chip breakage, which results in the smaller chip size (shown in Figure 5), contributing to the generation of many minor machining marks between major machining marks.

Surface Roughness

Two measurement methods, the contact profilometer and non-contact confocal microscopy, are utilized to measure the R_a of machined elastomer surfaces. Measurement results are summarized in Table 3. In confocal microscopy measurements, two sets of data with and without the FIR prefiltering are presented to explore the effect of different high frequency noise filtering procedures.

High spindle speed can improve the surface roughness. This is demonstrated in both profilometer and confocal microscope measurements. The same trend has been reported by Jin and Murakawa (4). It is obvious in Figure 12 that the high spindle speed increases the deformation rate and enables more frequent chip breakage and efficient cutting. The size of burrs is also much smaller on surfaces machined at 2400 rpm. Although high cutting speed can improve surface roughness, the smoke prohibits the high speed machining of elastomer in actual application. All tests at 2400 rpm have significantly visible smoke generated during machining.

The effect of workpiece cooling on surface roughness is not obvious. Unlike the distinctly different surface textures shown in the SEM

TABLE 3 Surface Roughness R_a Measured by the Stylus and Confocal Microscopy

		Room temperature tool			Induction-heated tool		
			Confocal microscopy			Confocal microscopy	
Spindle speed (rpm)	Workpiece temperature	Profilometer	No FIR pre-filtering	With FIR pre-filtering	Profilometer	No FIR pre-filtering	With FIR pre-filtering
1100	Room temperature	81.4	74.9	65.8	56.7	71.3	64.9
	Solid carbon dioxide cooled	76.9	71.0	65.0	54.6	70.4	62.8
2400	Room temperature	36.2	60.6	54.0	40.8	65.0	58.4
	Solid carbon dioxide cooled	39.3	64.5	57.1	36.8	59.9	53.0

micrographs in Figure 12, which also have the profilometer measured R_a values listed, the surface roughness R_a is about the same for workpiece machined with and without cryogenic cooling.

At 1100 rpm, the tool heating can reduce surface roughness. This is important because the elastomer machining at high spindle speed (2400 rpm) is not feasible due to smoke. Tool heating becomes an enabling method for precision machining of elastomer with good surface roughness. The tool heating at 1100 rpm also generate large groove width, as shown in Figure 11. This indicates that tool heating can enable more effective material removal and achieve better workpiece dimensional control at low cutting speed. For the carving of thread in prototype tire manufacturing, carvers use the heated, sharp blade to cut the elastomer at low speed. Heating the blade tool is critical to enable the cutting at a low speed. Similarly, induction heating the tool is important for low speed machining of elastomers.

Discrepancies exist between the profilometer and confocal microscope measurements. In general, the contact force at the stylus tip will deform the protruded fine features, such as burrs, on elastomer surface. Compared to the confocal microscope measurements, smaller R_a values are expected using the contact profilometer method. In Table 3, this is generally valid except on two surfaces machined at 1100 rpm without tool heating. As shown in Figure 12, these two surfaces have large burrs. The burr may bend and block the view of confocal microscope to reach the bottom of valley on machined surface. The low light reflectivity inside the valley may also limit the accuracy of surface roughness measurement using the confocal microscope. Both will result low R_a than the actual value.

The confocal microscope measurements are analyzed using the OmniSurf software to calculate the R_a. The data processed by OminSurf can be

pre-filtered using the FIR filter in MATLAB. Pre-filtering the data removes the noise as well as some fine features on surface measurement profile. It consistently lowers the R_a value. Although the pre-filtering changes the R_a value, it does not alter the general trend observed on the effect of cutting speed, workpiece cooling, and tool heating for surface roughness.

CONCLUSIONS

This study investigated effects of cutting speed, tool heating, and workpiece cooling on machining of elastomers. Cutting speed was demonstrated to be critical. At high cutting speed, smoke was generated and became environmentally hazardous. At low cutting speed, the surface roughness was high and material removal was not effective, which resulted in the narrow groove width in end milling. Induction heating the tool could improve the surface roughness and enable effective material removal for low speed machining of elastomers. On the chip morphology, high cutting speed and heated tool both promoted the generation of burned chip.

The frequency domain analysis of measured cutting forces revealed a consistent peak at about 7 Hz due to the vibration of low stiffness of elastomer workpiece during machining. Even using specially designed fixture to enclose every end milling cut, the low elastic modulus of elastomer stilled existed and affected the surface quality. On machined surface, the distance between major machining marks was correlated to the low frequency workpiece vibration.

Quantitative comparison of both contact stylus profilometer and noncontact confocal microscopy roughness measurements on machined elastomer surfaces were conducted. Both methods showed their limitations. The deformation of the fine surface features of elastomer using contact stylus resulted in lower R_a values compared to most of the confocal microscope measurements. Burrs on surface could block the view of confocal microscope to reach the bottom of valley. Low surface reflectivity inside the valley was also a problem. This study showed that the surface inspection of elastomers is still a technically challenging problem and requires further research.

Another future research area is the machining of precise three-dimensional shape of elastomer workpiece. The relatively small width of machined grooves, about 68 to 78% of the tool diameter, showed the difficulty to achieve good dimensional control of the elastomer workpiece. The induction-heated tool showed some improvement but was still not adequate for precise dimensional control. Novel methods need to be developed to further advance the elastomer machining technology and application.

ACKNOWLEDGMENTS

This research is sponsored by the National Science Foundation (DMI Grant #0099829) and Michelin Americas R&D Corp. Assistance provided by Jeffrey Gapczynski at DaimlerChrysler Co. and Marquis Alfonso at Siemens is gratefully acknowledged.

REFERENCES

[1] Shih, A.J., Lewis, M.A., and Strenkowski, J.S. (2004a). End Milling of Elastomers – Fixture Design and Tool Effectiveness for Material Removal. *Journal of Manufacturing Science and Engineering*, 126(1):115–123.

[2] Shih, A.J., Lewis, M.A., Luo, J., and Strnkowski, J.S. (2004b). Chip Morphology and Forces in End Milling of Elastomers. *Journal of Manufacturing Science and Engineering*, 126(1):124–130.

[3] Luo, J., Ding, H., and Shih, A.J. (2006). Induction-heated Tool Machining of Elastomers—Part I: Finite Difference Thermal Modeling and Experimental Validation. *Machining Science and Technology*, 9(4):547–565.

[4] Jin, M. and Murakawa, M. (1998). High-Speed Milling of Rubber (1st Report)–Fundamental Experiments and Considerations for Improvement of Work Accuracy. *Journal of the Japan Society for Precision Engineering*, 64(6):897–901.

[5] Berger, P. Michelin Americas R&D Corp., 2001, private communication.

[6] Stupak, P.R., Kang, J.H., and Donovan, J.A. (1990). Fractal Characteristics of Rubber Wear Surfaces as a Function of Load and Velocity. *Wear*, 141(1):73–84.

[7] Ganesan, L., Bhattacharyya, P., and Bhowmick, A.K. (1996). Quantitative Measurement of Roughness of Fractured Rubber Surfaces by an Image Processing Technique. *Journal of Materials Science*, 31(11):3043–3050.

[8] Schaal, S. and Coran, A.Y. (2000). Rheology and Processability of Tire Compounds. *Rubber Chemistry and Technology*, 73(2):225–239.

[9] Vardaxis, N.J. (1999). Confocal Scanning Laser Microscopy and Its Application in Biomedical Health Sciences. *Proceedings of the 1998 Research Workshop on New Approaches in Automated Medical Image Analysis*, Ballarat, Aust, Jul 31–Aug 1, 1998; Society of Photo-Optical Instrumentation Engineers, Bellingham, WA, USA, pp. 115–127.

[10] Smith, G.T. (2002). Surface Texture: Two Dimensional. In *Industrial Metrology: Surfaces and Roundness*, Springer, London, pp. 59–63.

[11] Whitehouse, D.J. (1994). Surface Characterization—The Nature of Surfaces and the Signals Obtained from them. In *Handbook of Surface Metrology*, Institute of Physics Publishing, London, pp. 5–102.

[12] Mark, J.E. (1996). Thermal-Oxidative Stability and Degradation of Polymers. In *Physical Properties of Polymers Handbook*, American Institute of Physics, New York, pp. 605–614.

[13] Harper, C.A. (1996). Fundamentals of Plastics and Elastomers. In *Handbook of Plastics, Elastomers, and Composites*, 3rd ed., McGraw-Hill, New York, pp. 1.75–1.88.

[14] Callister, W.D. (1997). Characteristics, Applications, and Processing of Polymers. In *Materials Science and Engineering An Introduction*, 4th ed., John Wiley & Sons, Inc., New York, pp. 465–505.

[15] Trent, E.M. (1991). Heat in Metal Cutting. In *Metal Cutting*, 3rd Ed. Butterworth Heinemann, Oxford, UK, pp. 57–85.

[16] Kim, C., Bono, M., and Ni, J. (2002). Experimental Analysis of Chip Formation in Micro-Milling. NAMRI XXX, West Lafayette, ID, May 21–24, Society of Manufacturing Engineers, 247–254.

[17] Sutherland, J.W. and Babin, T.S. (1988). The Geometry of Surfaces Generated by the Bottom of an End Mill. *Transaction of NAMRC*, 16:202–208.

[18] Luo, J. and Shih, A.J. (2005). Inverse Heat Transfer Solution of the Heat Flux Due to Induction Heating. *Journal of Manufacturing Science and Engineering*, 127(3):555–563.